NREL
NATIONAL RENEWABLE ENERGY LABORATORY

Models for Battery Reliability and Lifetime

K. Smith, E. Wood, S. Santhanagopalan, G.-H. Kim, J. Neubauer, and A. Pesaran

Presented at the Battery Congress 2013
Ann Arbor, Michigan
April 15-16, 2013

NREL is a national laboratory of the U.S. Department of Energy
Office of Energy Efficiency & Renewable Energy
Operated by the Alliance for Sustainable Energy, LLC

This report is available at no cost from the National Renewable Energy Laboratory (NREL) at www.nrel.gov/publications.

Conference Paper
NREL/CP-5400-57746
March 2014

Contract No. DE-AC36-08GO28308

This report is available at no cost from the National Renewable Energy Laboratory (NREL) at www.nrel.gov/publications.

Available electronically at http://www.osti.gov/scitech

Available for a processing fee to U.S. Department of Energy and its contractors, in paper, from:

U.S. Department of Energy
Office of Scientific and Technical Information
P.O. Box 62
Oak Ridge, TN 37831-0062
phone: 865.576.8401
fax: 865.576.5728
email: mailto:reports@adonis.osti.gov

Available for sale to the public, in paper, from:

U.S. Department of Commerce
National Technical Information Service
5285 Port Royal Road
Springfield, VA 22161
phone: 800.553.6847
fax: 703.605.6900
email: orders@ntis.fedworld.gov
online ordering: http://www.ntis.gov/help/ordermethods.aspx

Cover Photos: (left to right) photo by Pat Corkery, NREL 16416, photo from SunEdison, NREL 17423, photo by Pat Corkery, NREL 16560, photo by Dennis Schroeder, NREL 17613, photo by Dean Armstrong, NREL 17436, photo by Pat Corkery, NREL 17721.

Printed on paper containing at least 50% wastepaper, including 10% post consumer waste.

Models for Battery Reliability and Lifetime

Kandler Smith, Eric Wood, Shriram Santhanagopalan, Gi-Heon Kim, Jeremy Neubauer, Ahmad Pesaran
National Renewable Energy Laboratory

Abstract

Models describing battery degradation physics are needed to more accurately understand how battery usage and next-generation battery designs can be optimized for performance and lifetime. Such lifetime models may also reduce the cost of battery aging experiments and shorten the time required to validate battery lifetime. Models for chemical degradation and mechanical stress are reviewed. Experimental analysis of aging data from a commercial iron-phosphate lithium-ion (Li-ion) cell elucidates the relative importance of several mechanical stress-induced degradation mechanisms.

Introduction

Lifetime predictive models are needed to better understand design and operational consequences on performance degradation of Li-ion batteries (LIB). Calendar-life models describing LIB degradation have shown reasonable promise in predicting rate transport and reactions leading to lithium (Li) loss and can be closely matched to data (Ploehn, 2004; Safari, 2011). Detailed elementary chemical reaction models (Christensen, 2004; Colclasure, 2010) provide a framework for studying degradation reactions for different chemical systems. Cycle-life models of LIBs, however, have yet to offer a method to predict capacity fade for a wide range of cycling and environmental conditions. Coulombic-throughput or energy-throughput are sometimes used as proxies to describe mechanical stress-induced fade and are regressed to experimental capacity data (Peterson, 2010). These models are difficult to extend to a wide range of cycling conditions (Wang, 2010).

Mechanical stress has gained increasing attention in LIB modeling literature with one motivator being to create physical models of capacity fade that can help guide cell design. Mechanical stress effects have been modeled at length scales ranging from particle-level (Christensen, 2006) to electrode sandwich level (Renganathan, 2010; Xiao, 2010), cell level (Sahraei, 2012) and pack level (Sahari, 2010). Particle stress investigations have shown, for example, possible failure during fast-rate charging where intercalation-rate of Li into a negative electrode active particle drives a faster rate of expansion at the outer radii of the particle, generating high-tensile stress in the inner core that may lead to fracture. During de-intercalation, high-tensile stress occurs at the outside of the particle. Models predict theoretical stress levels below which no failure should occur, albeit for simplified electrode geometries without pre-existing flaws.

While these stress models already provide useful directional input to the design phase, further extensions are needed to predict capacity fade. Particle fracture models must be extended beyond crack initiation to describe crack propagation on a time scale relevant for life prediction. Computational models have not yet captured realistic geometries including dispersed flaws consequent of the manufacturing process. Fracture leading to apparent active-site isolation has been studied; however, additional factors that may lead to active-site isolation—such as binder failure coupled with differential expansion of various cell components—have not been studied as they relate to cycling fade rate. Cell and pack level models have mostly considered the impact of crush on various cell and pack geometries.

In this paper, we hypothesize a fatigue model to describe mechanical-stress-induced capacity fade. The model is regressed to capacity fade data from the literature for a commercial iron-phosphate cell. Based on the model, the relative importance of various mechanical-induced degradation mechanisms on cycle life is discussed.

Degradation Mechanism Hypotheses

Some important mechanical stress considerations leading to cell performance fade are illustrated in **Figure 1**. These are:

(i) Particle and electrode isolation caused by high-concentration, gradient-driven strains leading to fracture; rate is likely accelerated by high intercalation C-rates and low temperatures cycling

(ii) Particle and electrode isolation caused by loss of adhesive/cohesive properties leading to debonding of particles from one another, or delamination of active materials from current collectors; degradation rate acceleration factors likely include:
   a. High temperature leading to binder breakdown
   b. Depth-of-discharge (DOD) swings causing bulk strain of active materials
   c. Temperature swings during cycling and cool-down (ΔT) leading to differential strain amongst various cell components

(iii) External pressure and forcing conditions on the cell packaging transmitted to the jelly-roll; pressure supplied by a module housing, for example, can impact the cycle life of pouch cells.

For the present cylindrical cell tested in a laboratory environment, impact of external pressure and forcing can be neglected.

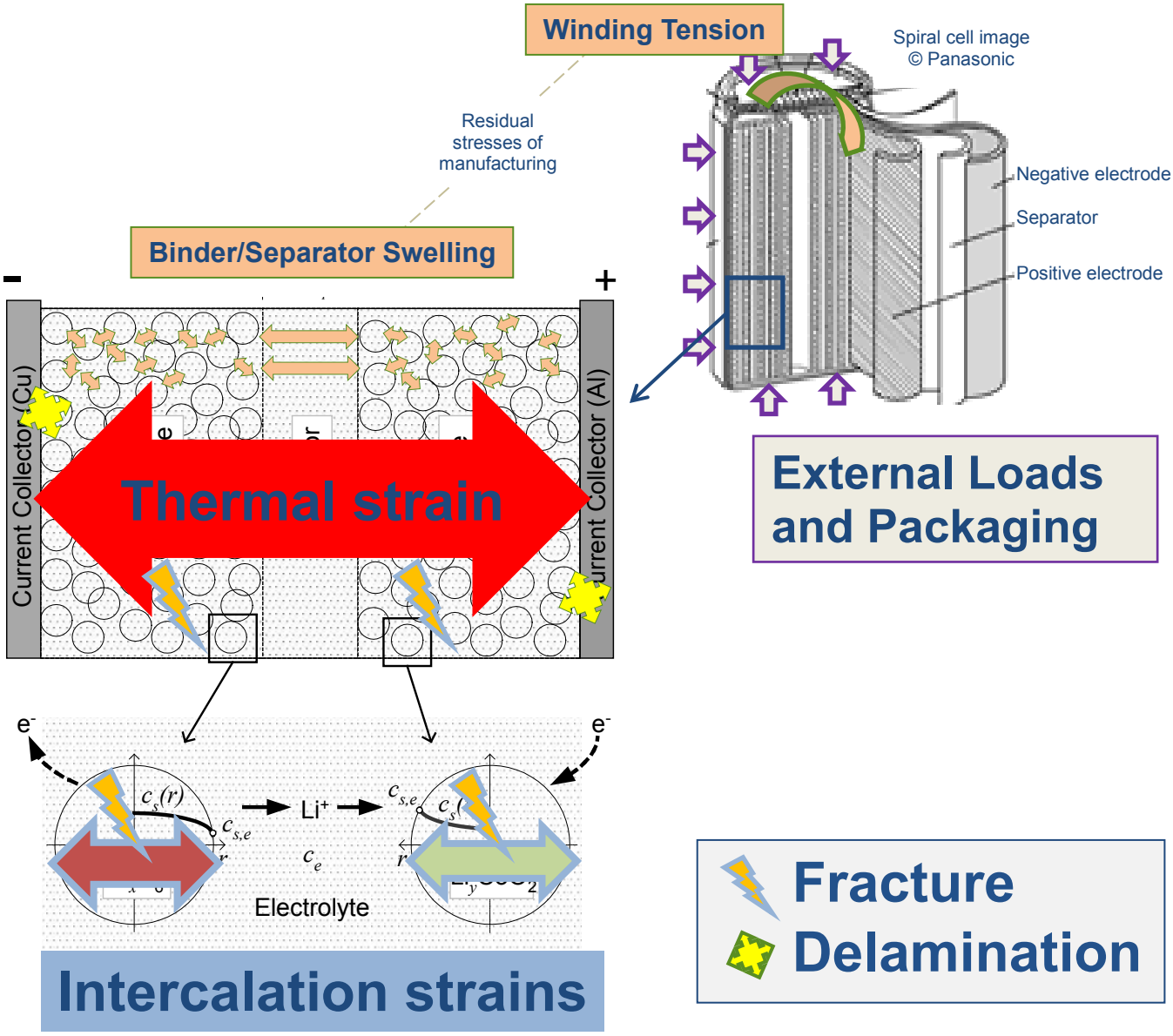

Fig. 1 Mechanical stress effects contributing to damage and performance fade

Mathematical Model

Estimation of relative effects of mechanical stress on capacity fade under different aging conditions is performed using a sequence of local model regression, degradation-rate visualization/hypothesis of rate functional form, and rate-law model regression. Local models and hypothesized rate laws are described below.

Local models

Local models describe capacity fade with time t and electro-thermo-mechanical cycles N for a single fixed aging condition. In the present model, relative capacity, q (available capacity at a given state-of-life divided by beginning-of-life capacity), is interpreted as

$$q = \min(q_{Li}, q_{sites}). \qquad [1]$$

where q_{Li} is capacity limited by cycleable-Li in the cell,

$$q_{Li} = b_0 + b_1 t^z + b_2 N, \; [2]$$

and q_{sites} is capacity limited by active-sites. Provided the cell is not stored in an over-discharged or over-charged state, we find q_{sites} predominantly correlates with number of cycles rather than time,

$$q_{sites} = c_0 + c_2 N. \qquad [3]$$

Equations [1-3] reproduce several common features observed in capacity fade data:

(i) Graceful fade regime observed for cells aged under pure storage conditions ($b_1 t^z$) or in low-to-moderate cycling conditions ($b_2 N$) in [2]

(ii) Linear fade regime ($c_2 N$) in [3] either observed
   a. immediately starting at BOL when a cell is repeatedly cycled at moderate-to-high stress levels such as during an accelerated cycling test, or if not then
   b. nearing EOL when an initial graceful fade region experiences a sudden knee where apparent capacity degradation suddenly accelerates.

The min function in Eq. [1] has several consequences for interpreting capacity fade data. First, multiple shapes of capacity versus age are possible. Second, depending on the chosen aging condition and extent of aging, degradation rates b_1, b_2, and c_2 may not all be observable from total capacity measurements for a single aging condition. To investigate mechanical stress degradation, the present paper only considers regression of a rate model for c_2 to data for the commercial graphite/iron-phosphate cell. Regression of parameters b_1 and b_2 will be described in a future publication.

Rate model

Tracking damage as a function of cycles N is common in fatigue literature. The fatigue approach used in the present work is practical when a mechanical-stress/life-predictive model must retain close relationship with supporting experimental data. Thermo-mechanical fatigue literature suggests formulas to combine effects of multiple simultaneous degradation mechanisms occurring in parallel. For gas turbine engines for example, the number of cycles to end-of-life (EOL) is expressed as harmonic mean of cycle-life for separate mechanisms

$$1/N_{EOL} = 1/N_{crack} + 1/N_{creep} + 1/N_{oxidation}. \qquad [4]$$

In [4], crack propagation is due to pure mechanical loading, creep is the flow of materials induced when mechanical cycles are superimposed with thermal cycles, and oxidation is material change due to accumulated exposure at high temperatures.

For a battery, one might hypothesize a similar model where life is limited by bulk DOD cycles, thermal cycles, and fracture driven by species concentration gradients

$$1/N_{EOL} = 1/N_{DOD} + 1/N_{\Delta T} + 1/N_{fracture}. \qquad [5]$$

Rationalizing this model with [3] implies that degradation rates, expressed as capacity fade per cycle, of the various mechanisms are additive

$$c_2 = c_{2,DOD} + c_{2,\Delta T} + c_{2,fracture}. \qquad [6]$$

The fatigue model must express the functional dependence of degradation rate on operating parameters, c_2 (DOD,ΔT,T,C_{rate},t_{pulse}). Consistent with the degradation mechanism hypotheses discussed above, we expect fracture degradation in [6] to be accelerated by sluggish intercalation at low temperatures (Safari, 2011), and high C-rates together with long (dis)charge times (Zhao, 2010). We propose a non-dimensional acceleration factor θ for intercalation-induced fracture,

$$\theta_{\text{intercal.}} = \exp\left(\frac{-E_a^{\text{intercal.}}}{\text{R}}\left(\frac{1}{T} - \frac{1}{T_{ref}}\right)\right)\left(\frac{C_{rate}}{C_{rate,ref}}\right)\left(\sqrt{\frac{t_{pulse}}{t_{pulse,ref}}}\right). \quad [7]$$

Binder breakdown is likely to lead to electrode site isolation, particularly for high temperature cycling. The capacity fade impact of binder failure is likely convoluted with occurrence of differential strain of particles, electrodes, and other cell components. A proposed capacity fade rate model describing binder degradation, differential expansion of cell components, and particle fracture effects is

$$c_2 = c_{2,ref}\left\{\exp\left(\frac{-E_a^{\text{binder}}}{R}\left(\frac{1}{T} - \frac{1}{T_{ref}}\right)\right)\left[m_1\, DOD + m_2\, \Delta T + m_3\, \theta^{\text{intercal.}}\right] + m_4\, \theta^{\text{intercal.}}\right\} \quad [8]$$

Several considerations are noted for regression of this rate model. As written, [8] is over-determined. Parameter m_1 is removed from the parameter search, given the constraint $m_1+m_2+m_3+m_4=1$. Next, it is difficult to regress two conflicting activation energies simultaneously. In [8], $E_a^{binder} > 0$ describes high temperature acceleration and $E_a^{intercal.} < 0$ describes low temperature acceleration. We fix activation energy for intercalation-induced fracture to $E_a^{intercal.} = 43321$ J/mol representing transport limitations in the graphite electrode (Safari, 2011) as studies have shown that particle damage is negligible for the iron-phosphate electrode with nano-sized particles.

The following section describes regression of parameters $p = [c_{2,ref},\ m_2,\ m_3,\ m_4,\ E_a^{binder}]$ in [8] and interpretation of mechanical stress-induced capacity fade created by this hypothesized model.

Data Regression Analysis

We compiled capacity fade data from multiple sources including Delacourt et al. (Safari 2011); HRL Labs consortium (Wang, 2010); and NASA Jet Propulsion Laboratory (Smart 2008). The total set of data encompasses 50 different aging conditions for a 2.2 Ah A123 26650 cell with graphite/iron phosphate chemistry.

In this work, we restrict our analysis to the knee regime of the capacity fade curves. **Figure 2** shows the subset of aging data within the apparent knee regime. Each tested condition is labeled according to the test laboratory, cycling profile and temperature, in the format "Lab, DOD, C-rate,dis/C-rate,chg, test chamber temperature." The knee regime is identified mathematically using thresholds for first and second derivatives of relative capacity, $dq/dt < 0$ and $d^2q/dt^2 < \varepsilon$ where ε is a small negative number.

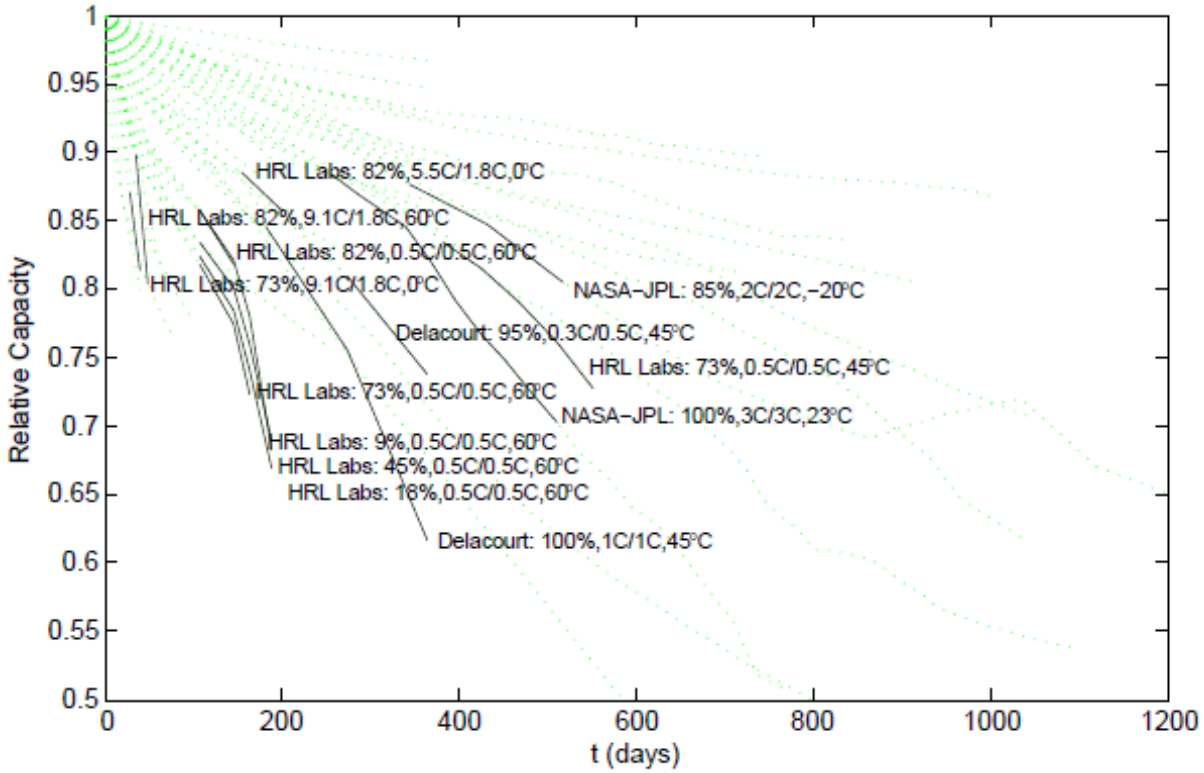

Fig. 2 Aging data for 2.2 Ah graphite/iron-phosphate cell; entire dataset (green dotted lines); subset of data in knee regime (black solid lines)

Local model regression

A value of parameter $p = [c_2]$ in [3] is regressed to fit the knee region in each of the 13 datasets, creating 13 rate values that can be visualized for dependence on temperature and cycling condition. In [3] we assume $c_0 = 1$ which, for the present cell, is supported by the data. Local model fits to capacity fade trajectories are shown in **Figure 3**. The combined models capture the knee-region of capacity fade with 1.37% root-mean-square error (RMSE). . The rate of capacity fade, c_2, for each aging condition is shown in **Figure 4** versus the inverse of temperature. Confidence intervals are narrow in most cases. High C-rate cycling at 0°C is not estimated as well. This could be partly attributable to error in the thermal model we employed to estimate $T(t)$ for each aging condition, together with the assumption that associated duty-cycle stress variables T and ΔT stay constant throughout life.

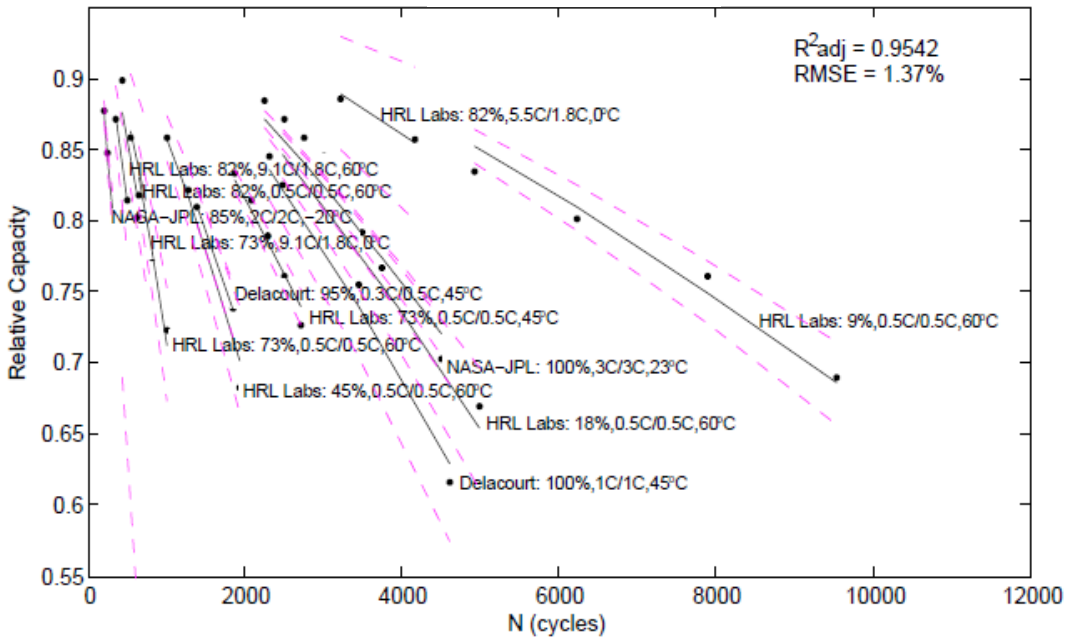

Fig. 3 Local model [3] fit to 13 separate data sets; data (·), model (-), 95% confidence intervals (--)

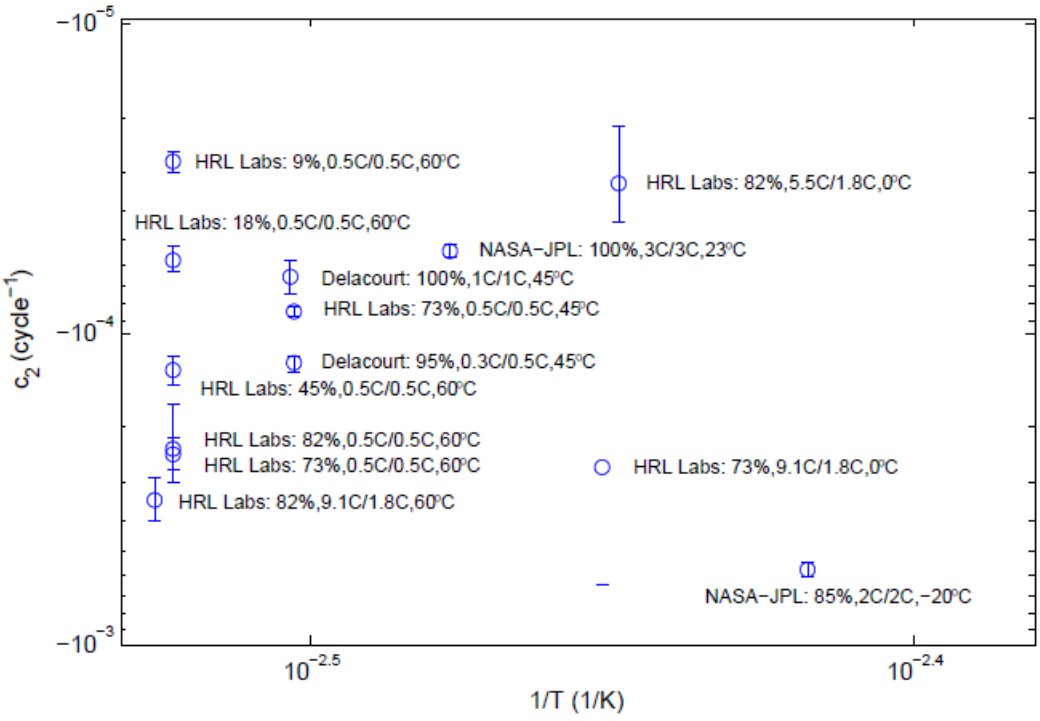

Fig. 4 Capacity fade rate determined by local model fits [3] for 13 tested aging conditions; error bars are 95% confidence intervals for parameter c_2 (they relate to confidence intervals in Fig 3)

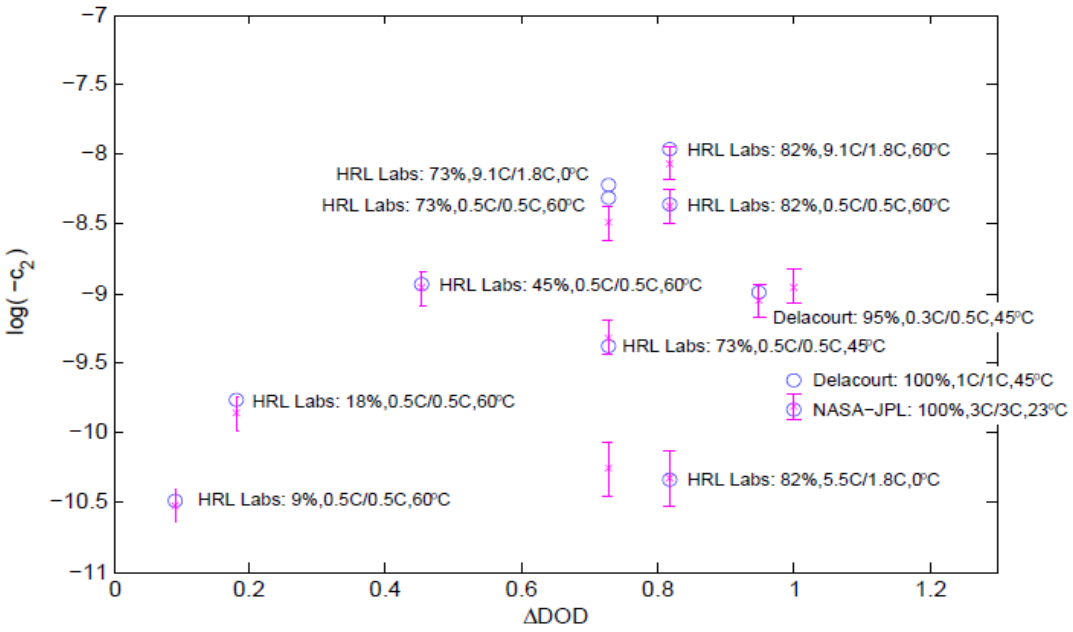

Fig. 5 Capacity fade rate; rates from local models (blue "o") and global rate-law model [7-8] (purple "x", together with confidence intervals of global model)

Rate model regression

Although not shown here, the proposed global rate-law model [7-8] cannot represent the NASA-JPL 2C/2C, -20°C test condition well with reasonable parameter values. It is possible that this cell's steep fade trajectory is controlled by Li plating rather than active site loss. Li plating is a likely side reaction to occur at low temperatures and high charge C-rates, such as for this test condition. We do not include this test condition when fitting the global rate-law model. Also not discussed further, over the course of our investigation we compared numerous alternate model forms to that described here. This paper only describes the most plausible model [7-8].

Simultaneous regression of parameters $p = [c_{2,ref}, m_2, m_3, m_4, E_a^{binder}]$ is challenging for traditional non-linear regression tools, such as the Levenberg-Marquardt algorithm used here. Though sub-optimal, by separately fitting different regions of the data (e.g., low C-rates and limited temperature ranges) we find E_a^{binder} has a value of around 36,000 to 53,000 J/mol. A typical median value that represents the entire dataset well is 49000 J/mol. Parameters m_2, m_3, and m_4 are determined by direct search, stepping through the parameter space between 0 and 1 for each m_i while regressing $c_{2,ref}$, sometimes in combination with other parameters. The best model fit identified uses $m_1 = 0.83$, $m_2 = 0.04$, $m_3 = 0$, $m_4 = 0.13$ with quality of fit $R^2 = 0.96$.

Figure 5 compares the global rate-law prediction with rates estimated from regression of local models. While the data may be less than optimally fit—a subject of future effort—the hypothesized model and parameters offer interesting physical interpretation. Reference conditions used in [7-8] are T_{ref}= 23°C, $C_{rate,ref}$ = 1C, DOD_{ref} = 100%. The parameters m_i thus imply that, under typical cycling conditions of 100% DOD, 1C charge and discharge at room temperature:

- 83% of active site loss is attributed to bulk volumetric expansion/contraction of the active material
- 4% of active site loss is attributed to temperature swings encountered by the cell
- 13% of active site loss is attributed to particle fracture owing to intercalation stress at high C-rates.

These ratios will change depending on temperature and cycling condition.

Conclusions

While conclusions are tentative pending validation with further data, the hypothesized fatigue model and analysis of graphite/iron-phosphate aging data suggests that some 83% of mechanical-induced active-site loss is attributable to bulk DOD swings during cycling. As the iron-phosphate electrode is made with mechanically stable nano-sized particles, we attribute the expansion/contraction-driven site loss to the graphite electrode with micron-sized particles. The present model partially supports the use of Amp-hour throughput as a proxy for modeling capacity fade due to site loss, since the product of *DOD* with number of cycles *N* relates directly to Amp-hour throughput. This work extends Amp-hour throughput models to include the effects of C-rate, temperature, and—also importantly—calendar fade.

While DOD swings apparently cause the most damage, we estimate that C-rate-driven particle fracture contributes on the order of 13% to active site loss. The model and data further estimate that temperature swings, causing differential thermal expansion of cell components, contributes weakly on the order of 4% to active site loss. The presented fatigue model, while simple, provides a relatively robust description of the 2.2 Ah cylindrical graphite/iron-phosphate cell life data. It will be applied in future work within a more sophisticated multi-dimensional physical degradation model framework.

Acknowledgements

The authors gratefully acknowledge funding by U.S. Department of Energy Office of Vehicle Technologies - Energy Storage, program managers David Howell and Brian Cunningham, and U.S. Army Tank Automotive Research, Development and Engineering Center, program manager Yi Ding.

References

1. J. Christensen, J. Newman, "A mathematical model for the lithium-ion negative electrode solid electrolyte interphase," J. Echem. Soc. (2004) 151 (11) A1977-1988
2. H.J. Ploehn, R. Premanand, R.E.White, "Solvent diffusion model for aging of lithium-ion battery cells," J. Echem. Soc. (2004) 151 (3) A456-A462
3. M. Safari, C. Delacourt, "Simulation-based analysis of aging phenomena in a commercial graphite/LiFePO4 cell," J. Echem. Soc. (2011) 158 (12) A1436-1447
4. S.B. Peterson, J. Apt, J.F. Whitacre, "Lithium-ion battery cell degradation resulting from realistic vehicle and vehicle-to-grid utilization," J. Power Sources (2010) 195, 2385-2393
5. J. Wang, P. Liu, J. Hicks-Garner, E. Sherman, S. Soukiazian, M. Verbrugge, H. Tataria, J. Musser, P. Finamore, "Cycle-life model for graphite-LiFePO4 cells," J. Power Sources (2011) 196, 3942-3948
6. M. Safari, C. Delacourt, "Mathematical modeling of lithium iron phosphate electrode: Galvanostatic charge/discharge path dependence," J. Echem. Soc. (2011) 158 (2) A63-73
7. J. Christensen, J. Newman, "A mathematical model of stress generation and fracture in lithium manganese oxide," J. Echem. Soc. (2006) 153 (6) A1019-1030
8. S. Renganathan, G. Sikha, S. Santhanagopalan, R.E. White, "Theoretical analysis of stresses in a lithium ion cell," J. Echem. Soc. (2010) 157 (2) A155-163
9. X. Xiao, W. Wu, X. Huang, "A multi-scale approach for the stress analysis of polymeric separators in a lithium-ion battery," J. Power Sources (2010) 195, 7649-7660
10. E. Sahraei, R. Hill, T. Wierzbicki, "Calibration and finite element simulation of pouch lithium-ion batteries for mechanical integrity," J. Power Sources, (2012) 201, 307-321
11. E. Sahraei, R. Hill, T. Wierzbicki, "Modeling and short circuit detection of 18650 Li-ion cells under mechanical abuse conditions," J. Power Sources, (2012) 201, 307-321
12. E. Sahraei, R. Hill, T. Wierzbicki)Modeling of lithium-ion batteries for crash safety," Global Powertrain Congress, Troy, Michigan, Nov. 4, 2010.
13. K. Zhao, M. Pharr, J.J. Vlassak, Z. Suo, "Fracture of electrodes in lithium-ion batteries caused by fast-charging," J. Appl. Phys (2010) 108, 073517
14. M.C. Smart, R.V. Bugga, L. Whitcanack, A.S. Gozdz, S. Mani, "Improved low temperature performance of high rate nano-lithium iron phosphate-based Li-ion cells with advanced electrolytes," 214th Echem. Soc. Mtg., Honolulu, Hawaii, October 15, 2008